Available online at www.sciencedirect.com

SciVerse ScienceDirect

Ceramics International 38 (2012) 1771–1777

CERAMICS INTERNATIONAL

www.elsevier.com/locate/ceramint

Effect of calcination temperature on structural, vibrational, optical, and rheological properties of zirconia nanoparticles

Elaheh K. Goharshadi [a,b,*], Mahboobeh Hadadian [a]

[a] Department of Chemistry, Ferdowsi University of Mashhad, Mashhad 91779, Iran
[b] Center of Nano Research, Ferdowsi University of Mashhad, Iran

Received 13 August 2011; received in revised form 28 September 2011; accepted 29 September 2011
Available online 6 October 2011

Abstract

ZrO_2 nanoparticles (NPs) were prepared by a simple, versatile, and an efficient methodology based on microwave. The synthesized NPs were calcined at temperatures ranging from 100 °C to 600 °C. The samples were characterized by X-ray powder diffraction (XRD), transmission electron microscope (TEM), FT-IR spectroscopy, Far-IR spectroscopy, Raman spectroscopy, and UV-vis absorption spectroscopy. The results clearly showed the presence of purely monoclinic phase of zirconia when the calcination temperature exceeds 400 °C. The experimental results showed that the viscosity of zirconia NPs in ethylene glycol (EG) increases with increasing the particle volume fraction and decreases with increasing temperature.

© 2011 Elsevier Ltd and Techna Group S.r.l. All rights reserved.

Keywords: Zirconia nanoparticle; Calcination temperature; Nanofluid; Viscosity

1. Introduction

Zirconia (zirconium oxide, ZrO_2) NPs are attracting increasing interest because of a number of key characteristics. These include excellent chemical resistance, refractory character, relatively high electronic conductivity, high oxygen ion conductivity, good mechanical strength, relatively high thermal expansion coefficient, good thermal stability, high fracture toughness and hardness, and high refractive index [1–3]. These unique properties are yet to be tapped for a large number of industrial applications [4–8].

At ambient pressure, zirconia has three polymorphs including monoclinic, tetragonal, and cubic depending on the temperature. The monoclinic form is thermodynamically stable at room temperature but transforms reversibly to the tetragonal structure above 1170 °C. This transformation is accompanied by volume shrinkage of 3–5%. The stable structure above 2370 °C is cubic [9].

A variety of methods have been applied to fabricate zirconia NPs such as precipitation method [1], sol–gel processing [10–12], chemical vapor synthesis [13], microwave plasma synthesis [14], inert gas condensation [15], combustion synthesis [16], ultrasonically assisted hydrothermal synthesis [17], laser ablation [18], autoclave method [19], microwave approach [6], ball milling [20], microemulsion methods [21–23], and hydrothermal treatments [24,25].

Among these preparation methods, microwave has the advantages of volumetric heating and the consequent dramatic increase in reaction rates, high-efficiency, high purity, and formation of nanoparticles with a narrow size distribution, and no serious agglomeration [26].

In the present study, we employed the microwave method to prepare the zirconia NPs. The structural, vibrational, and optical properties of the zirconia NPs were determined in depth with XRD, TEM, FT-IR spectroscopy, Far-IR spectroscopy, Raman spectroscopy, and UV-vis absorption spectroscopy. The dispersion behavior of zirconia nanoparticles in deionized water was investigated at different pH by the method of zeta potential. The experimental results of the effect of temperature, shear rate, and volume fraction on the viscosity of zirconia–EG nanofluids were reported.

* Corresponding author at: Department of Chemistry, Ferdowsi University of Mashhad, Mashhad 91779, Iran. Tel.: +98 511 8797022x308; fax: +98 511 8796416.
E-mail address: gohari@ferdowsi.um.ac.ir (E.K. Goharshadi).

0272-8842/$36.00 © 2011 Elsevier Ltd and Techna Group S.r.l. All rights reserved.
doi:10.1016/j.ceramint.2011.09.063

2. Materials and methods

2.1. Materials

All chemicals used were of analytical grade and used as received without further purification.

2.2. Experimental

The ZrO_2 nanoparticles were synthesized via the hydrolysis of zirconyl nitrate in aqueous–alcohol solution using microwave irradiation. In details, 50 ml of 0.2 M $ZrO(NO_3)_2$ aqueous solution was mixed with 200 ml tert-butyl alcohol. Then, the mixture was placed in microwave oven and heated to the boiling point for 3 min. After adding 25% ammonia to the mixture in order to prevent the precipitate formed in the course of microwave hydrolysis from being dissolved on cooling, the precipitate was centrifuged, washed with deionized water, and dried at 60 °C for 1 h. The obtained solid was calcined at different temperatures between 100 °C and 600 °C for 5 h.

The nanoparticles of zirconia were dispersed in EG by applying ultrasonic processor (Sonicator 4000) for 30 min. The frequency of ultrasound wave is 20 kHz. The total acoustic power injected into the solution was found to be 700 W. The volume fraction of nanofluids was varied from 0.0.1% to 0.04%.

2.3. Characterization techniques

The powder phases were determined by means of a Bruker/D8 Advanced diffractometer in the 2θ range from 20° to 80°, by step of 0.04°, with graphite monochromatic Cu Kα radiation (λ = 1.541 Å). The TEM analyses of the samples were done using a LEO 912 AB instrument. The electron beam accelerating voltage was 120 kV.

The Fourier transform infrared spectra of the fabricated zirconia NPs were recorded at room temperature with a KBr pellet on a Shimadzu 4300 Spectrometer ranging from 450 to 4000 cm^{-1}. The Far-IR spectra in the region 600–250 cm^{-1} were obtained using a Thermo Nicolet NEXUS 870 FT-IR spectrometer equipped with DTGS/polyethylene detector and a solid substrate beam splitter. The spectra were collected with a resolution of 4 cm^{-1}.

The FT-Raman spectra in the region 700–200 cm^{-1} were recorded employing a 180° back-scattering geometry and a Bomem MB-154 Fourier transform Raman spectrometer operating at the 1064 nm excitation line of a Nd:YAG laser. It was equipped with a ZnSe beam splitter and a TE cooled InGaAs detector. The spectra were accumulated for 1500 scans with a resolution of 2 cm^{-1}.

The UV–vis absorbance spectra were obtained for the samples using an Agilent photodiode-array Model 8453 equipped with glass of 1 cm path length. The spectra were recorded at room temperature in air within the range 200–600 nm.

The zeta potential of the zirconia NPs in deionized water was measured by the Zetasizer (Nano-ZS) from Malvern instrument.

The viscosity of the nanofluids of zirconia NPs in EG was measured using a Brookfield Viscometer (LV DV-II + Pro EXTRA) with a small sample adaptor.

3. Results and discussion

3.1. Characterization

Fig. 1 shows the XRD patterns of zirconia samples calcined at different temperatures. The XRD patterns illustrate that the sample without calcination as well as those calcined at 100 and 300 °C are amorphous forms. Increasing the calcination temperature, the amorphous phase transforms to monoclinic phase at 400 °C. The average crystallite size of the monoclinic zirconia was estimated using the Scherrer formula:

$$D_{hkl} = \frac{k \times \lambda}{\beta_{hkl} \times \cos\theta_{hkl}} \quad (1)$$

where D_{hkl} is the particle size perpendicular to the normal line of (h k l) plane, k is a constant (0.9), β_{hkl} is the full width at half maximum of the (h k l) diffraction peak, θ_{hkl} is the Bragg angle of (h k l) peak and λ is the wavelength of X-ray. The characteristics of the nanozirconia samples from XRD patterns were summarized in Table 1. Table 1 shows the average crystallite size was about 20 nm. When the calcination temperature increases above 400 °C, there is no significant difference among the samples.

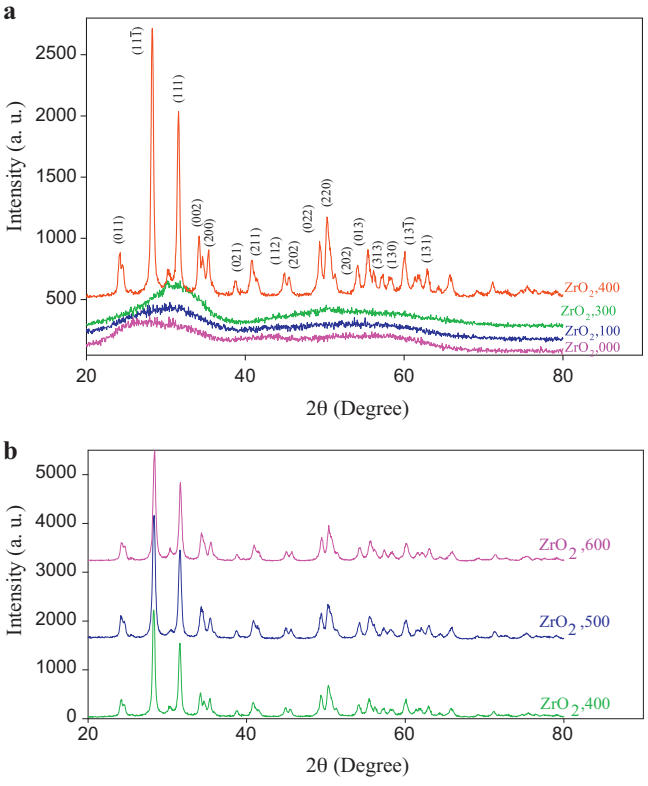

Fig. 1. The XRD pattern of zirconia NPs for: (a) ZrO_2,000 (without calcination), ZrO_2,100 (calcined at 100 °C), ZrO_2,300, and ZrO_2,400; (b) ZrO_2,400, ZrO_2,500, and ZrO_2,600.

Table 1
The characteristics of the samples from XRD patterns.

Sample	$D_{11\bar{1}}$ (nm)	D_{111} (nm)	$D_{13\bar{1}}$ (nm)
ZrO_2,400	23.01	22.86	20.44
ZrO_2,500	19.76	20.11	15.77
ZrO_2,600	21.60	22.10	16.70

Typical TEM images of sample ZrO_2,500 was shown in Fig. 2 with two magnifications. The average particle size of particles is about 27 nm.

Fig. 3(a) and (b) show the FT-IR spectra of the samples. The broad band at ca. 3400 cm^{-1} and the small band at 1600 cm^{-1} correspond to the physically adsorbed water on the samples. The band at around 1380 cm^{-1} is attributed to atmospheric CO_2. The absorption bands observed at approximately 500, 580, and 740 cm^{-1} for monoclinic zirconia conform fairly well with those reported by Debsikdar [27]. The active modes increase markedly upon lowering the symmetry of the structure by going from cubic to tetragonal and then to monoclinic ZrO_2. In contrast to the multiple absorption bands observed at low-frequency region for the monoclinic zirconia, no significant band was detected for the tetragonal zirconia in this region [28].

Fig. 3(c) displays the Far-IR spectra of two samples calcined at 500 and 600 °C. These spectra conform obviously the monoclinic phase as the FT-IR spectra.

Raman spectra can discriminate between the polymorph forms of the zirconia NPs [29]. The Raman spectra presented in Fig. 4 shows the lines at 304, 345, 475, 559, and 636 cm^{-1} can be attributed to A_g modes and 222, 332, 381, 502, 536, and 617 cm^{-1} can be assigned to B_g modes of monoclinic zirconia for samples calcined at 500 and 600 °C. Fig. 4 also shows other systems are amorphous. Hence, Raman spectra confirm the observation made by X-ray diffraction technique and IR spectroscopy: only monoclinic zirconia NPs are formed when the temperature of calcination exceeds 400 °C in this work.

The zeta potential of colloidal dispersions of ZrO_2,500 (Fig. 5) in water at different pH values was measured. The isoelectric point was found to be at pH 3.6.

3.2. Optical properties

Fig. 6 displays the UV–vis absorption spectrum of ZrO_2,000. All the samples distinctly showed a strong absorption band around 200 nm in wavelength at the UV region.

Zirconia is a large band gap semiconductor [30]. The optical band gap, E_g, can be determined from Tauc's equation [31,32] shown in the inset of Fig. 6:

$$(\alpha h\upsilon)^2 = B(h\upsilon - E_g) \quad (2)$$

where $h\upsilon$ is the photon energy, α is the absorption coefficient, and B is a constant relative to the material. The values of band gap energy and the maximum absorption wavelength of the samples were summarized in Table 2. The optical band gap of bulk monoclinic zirconia is 5 eV [30].

3.3. The rheological data

The equation governing Newtonian behavior of a fluid is given by:

$$\tau = \eta\gamma^{\circ} \quad (3)$$

where τ is the shear stress, η is the shear viscosity, and γ° is the shear rate. As Fig. 7 shows EG acts as a Newtonian fluid.

There was no any difference among the rheological properties of different samples. The viscosity of nanofluids of zirconia NPs (ZrO_2,500) in EG as a base fluid was measured at different volume fractions (0.01%, 0.02%, and 0.04%) and different temperatures (25, 35, and 45 °C). As Fig. 8 shows the viscosity of nanofluids depends upon shear rate and therefore the nanofluids are non-Newtonian fluids. Hence, Newtonian behavior of EG changes to non-Newtonian for nanofluids because of the interactions between the fluid and NPs [33]. Clearly, as shear rate increases, this effect becomes less marked, suggesting that interactions are relatively weak and broken down at high shear rates. As Figs. 7 and 8 show the viscosity decreases with increasing temperature.

The viscosity of nanofluids increases with increasing the volume fraction (Fig. 9). As the volume fraction increases, the number of NPs increases. It causes the fluid becomes less mobilized and hence the viscosity increases.

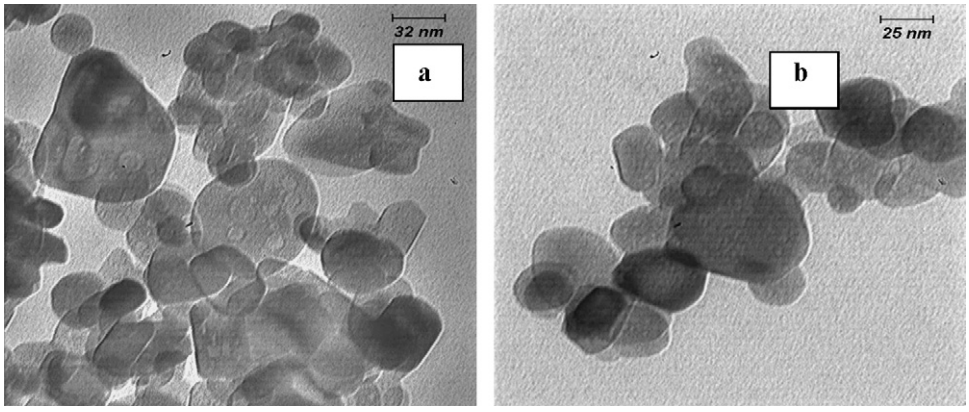

Fig. 2. The TEM image of sample ZrO_2,500 with two magnifications.

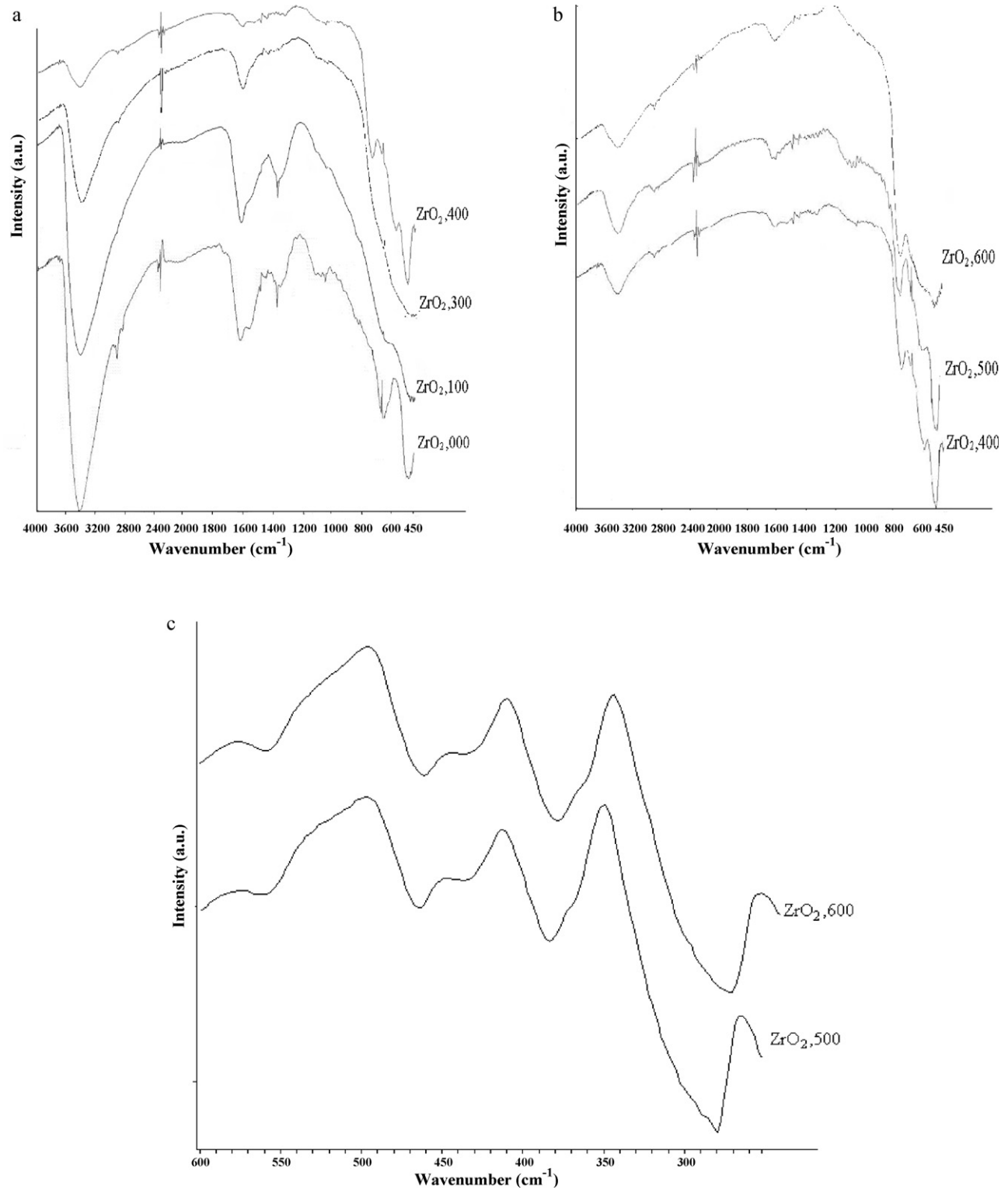

Fig. 3. The FT-IR spectra for: (a) ZrO_2,000, ZrO_2,100, ZrO_2,300, and ZrO_2,400; (b) ZrO_2,400, ZrO_2,500, and ZrO_2,600; (c) The Far-IR spectra of zirconia NPs for ZrO_2,500, and ZrO_2,600.

The temperature dependence of viscosity of nanofluids is reasonably described by Vogel–Fulcher–Tammann (VFT) equation [34,35]:

$$\eta(T) = A \exp\left(\frac{B}{T + T_0}\right) \quad (4)$$

where η is the shear viscosity of nanofluid, parameter B is related to the free activation energy of fluid, and A and T_0 are fitting parameters. The experimental data at a constant shear rate were fitted by Eq. (4) and the results were shown in Fig. 10. The fitting parameters and the discrepancy between the fitted data and the measurements were summarized in Table 3.

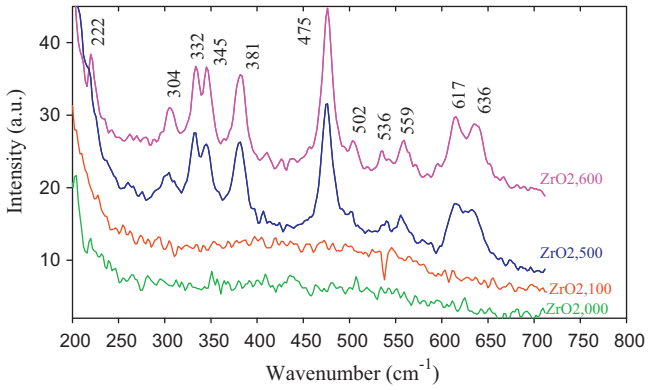

Fig. 4. The Raman spectra of zirconia NPs for samples.

Table 2
The optical properties of the samples.

Sample	E_g (eV)	λ_{max} (nm)
ZrO_2,000	5.45	205
ZrO_2,100	5.50	204
ZrO_2,300	5.48	204
ZrO_2,400	5.56	202
ZrO_2,500	5.49	204
ZrO_2,600	5.58	201

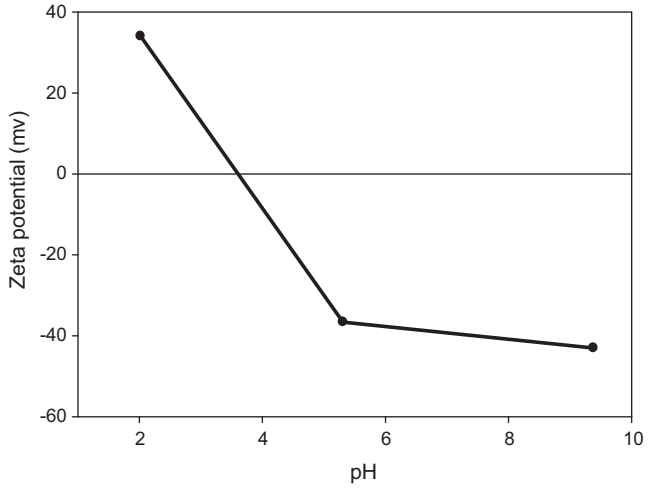

Fig. 5. The zeta potential of zirconia NPs (ZrO_2,500) dispersed in deionized water under various pH values.

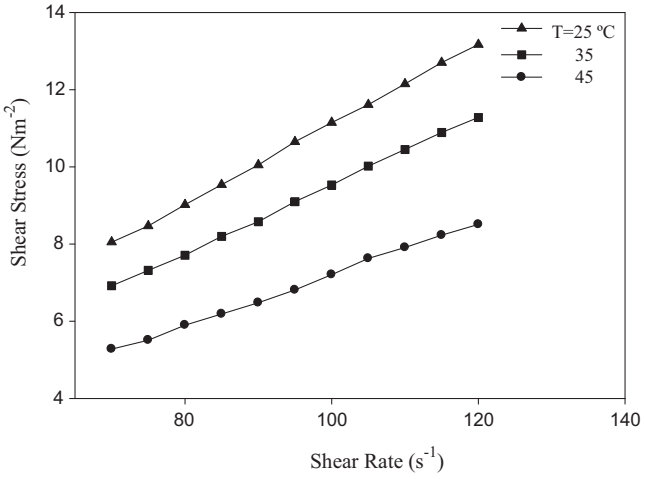

Fig. 7. Shear stress versus shear rate for EG at different temperatures.

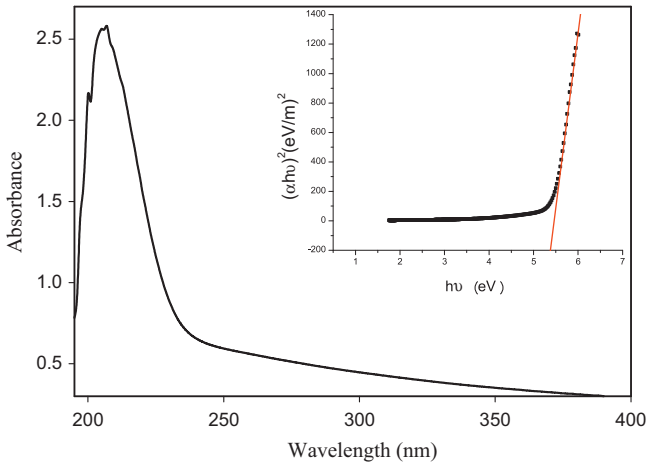

Fig. 6. The UV–vis spectrum of ZrO_2,000 sample dispersed in ethanol. Plot of $(\alpha h\upsilon)^2$ vs. photon energy (inset).

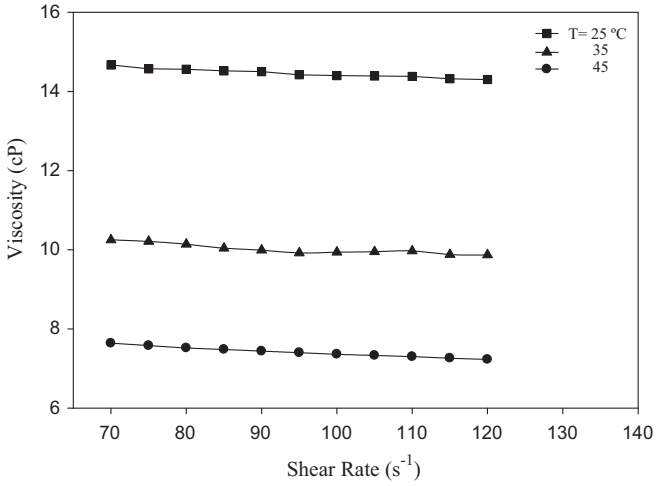

Fig. 8. Viscosity versus shear rate for zirconia–EG nanofluids ($\phi = 0.01\%$) at different temperatures.

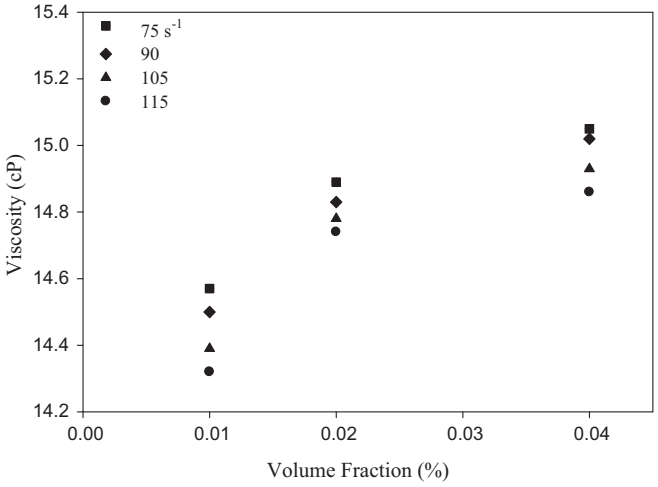

Fig. 9. Viscosity of zirconia–EG nanofluids as a function of volume fractions at different shear rates at 25 °C.

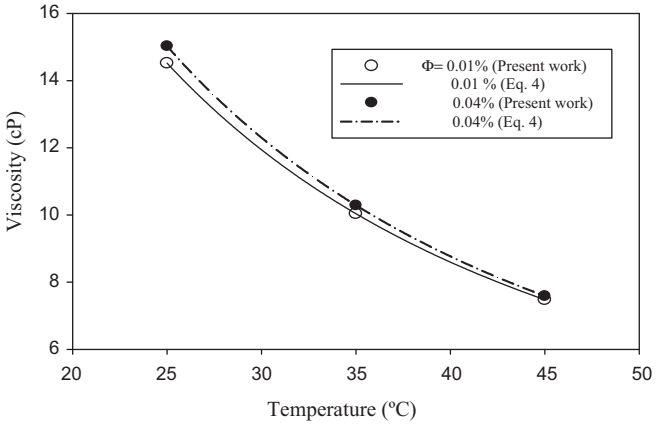

Fig. 10. Viscosity of zirconia–EG nanofluids as a function of temperature at a constant shear rate (85 s^{-1}), the symbols and lines are the measured and calculated values using Eq. (4), respectively.

Table 3
The empirical constants of Eq. (4) and the mean deviation (D_m) between the equation and measurements.

Sample	A	B	T_0	D_m
ZrO_2 + EG ($\Phi = 0.01\%$, $\gamma^\circ = 85\ s^{-1}$)	0.5462	258.8313	53.9068	0.0082
ZrO_2 + EG ($\Phi = 0.04\%$, $\gamma^\circ = 85\ s^{-1}$)	0.4663	283.6146	56.6642	0.0038

4. Conclusions

It seems to us the following important conclusions can be drawn from the present study:

1. The zirconia NPs were successfully synthesized using microwave method without using any surfactant. The samples were characterized using different techniques. All of the techniques confirmed the presence of nearly pure monoclinic nanocrystals when the calcination temperature was above 400 °C.
2. The rheological properties of zirconia–EG nanofluids as functions of shear rate, volume fraction, and temperature were measured.
3. Although the base fluid, EG, acts as a Newtonian fluid, the nanofluid of zirconia–EG behaves as non-Newtonian fluid at low shear rates.

Acknowledgments

The authors express their gratitude to Ferdowsi University of Mashhad for support of this project (15832/3). The authors would also like to acknowledge Professor Sayyed Faramarz Tayyari for taking the Far-IR and Raman spectra and Mrs. Roksana Pesian for taking TEM images.

References

[1] A.P. Oliveira, M.L. Torem, The influence of precipitation variables on zirconia powder synthesis, Powder Technol. 119 (2001) 181–193.
[2] G.Y. Guo, Y.L. Chen, A nearly pure monoclinic nanocrystalline zirconia, J. Solid State Chem. 178 (2005) 1675–1682.
[3] M. Tahmasebpour, A.A. Babaluo, M.K. Razavi Aghjeh, Synthesis of zirconia nanopowders from various zirconium salts via polyacrylamide gel method, J. Eur. Ceram. Soc. 28 (2008) 773–778.
[4] W.R. Cannon, E. Gugel, G. Leimer, G. Woetting, Advanced structural products, in: Ulmann's Encyclopedia of Industrial Chemistry, Wiley-VCH Verlag, 2002.
[5] H. Sui, L. Zhang, W. Zong, Synthesis and characterization of nanozirconium dioxide in recombination surfactant association system, J. Dispers. Sci. Technol. 28 (2007) 1316–1324.
[6] K.P.S.S. Hembram, G. Mohan Rao, Microwave synthesis of zirconia nanoparticles, J. Nanosci. Nanotechnol. 8 (2008) 4159–4162.
[7] L. Li, P. Zhang, J. Liang, S.M. Guo, Phase transformation and morphological evolution of electrospun zirconia nanofibers during thermal annealing, Ceram. Int. 36 (2010) 589–594.
[8] N. Chandra, D.K. Singh, M. Sharma, R.K. Upadhyay, S.S. Amritphale, S.K. Sanghi, Synthesis and characterization of nano-sized zirconia powder synthesized by single emulsion-assisted direct precipitation, J. Colloid Interface Sci. 342 (2010) 327–332.
[9] D. Bloor, R.J. Brook, M.C. Flemings, S. Mahajan (Eds.), Encyclopedia of Advanced Materials, Elsevier Science Ltd, 1994, p. 2965.
[10] C. Stocker, A. Baiker, Zirconia aerogels: effect of acid-to-alkoxide ratio alcoholic solvent and supercritical drying method on structural properties, J. Non-Cryst. Solids 223 (1998) 165–178.
[11] I.I. Stefanc, S. Music, G. Stefanic, A. Gajovic, Thermal behavior of ZrO_2 precursors obtained by sol–gel processing, J. Mol. Struct. 480 (1999) 621–625.
[12] J.A. Wang, M.A. Valenzuela, J. Salmones, A. Vazquez, A. Garcia-Ruiz, X. Bokhimi, Comparative study of nanocrystalline zirconia prepared by precipitation and sol–gel methods, Catal. Today 68 (2001) 21–30.
[13] V.V. Srdic, M. Winterer, Comparison of nanosized zirconia synthesized by gas and liquid phase methods, J. Eur. Ceram. Soc. 26 (2006) 3145–3151.
[14] D. Vollath, K.E. Sickafus, Synthesis of nanosized ceramic oxide powders by microwave plasma reactions, Nanostruct. Mater. 1 (1992) 427–437.
[15] R. Nitsche, M. Rodewald, G. Skandan, H. Fuess, H. Hahn, Hrtem study of nanocrystalline zirconia powders, Nanostruct. Mater. 7 (1996) 535–546.
[16] R.D. Purohit, S. Saha, A.K. Tyagi, Combustion synthesis of nanocrystalline ZrO_2 powder: XRD Raman spectroscopy and TEM studies, Mater. Sci. Eng. B 130 (2006) 57–60.
[17] P.E. Meskin, V.K. Ivanov, A.E. Barantchikov, B.R. Churagulov, Y.D. Tretyakov, Ultrasonically assisted hydrothermal synthesis of nanocrystalline ZrO_2, TiO_2 $NiFe_2O_4$ and $Ni_{0.5}Zn_{0.5}Fe_2O_4$ powders, Ultrason. Sonochem. 13 (2006) 47–53.

[18] H.Y. Lee, W. Riehemann, B.L. Mordike, Sintering of nanocrystalline ZrO_2 and zirconia toughened alumina (ZTA), J. Eur. Ceram. Soc. 10 (1992) 245–253.
[19] F.J. Berry, S.J. Skinner, I.M. Bell, R.J.H. Clark, C.B. Ponton, The influence of pH on zirconia formed from Zirconium(IV) acetate solution: characterization by X-ray powder diffraction and Raman spectroscopy, J. Solid State Chem. 145 (1999) 394–400.
[20] M. Gateshki, V. Petkov, G. Williams, S.K. Pradhan, Y. Ren, Atomic-scale structure of nanocrystalline ZrO_2 prepared by high-energy ball milling, Phys. Rev. B 71 (2005) 224107–2241016.
[21] C.Y. Tai, B.Y. Hsiao, H.Y. Chiu, Preparation of silazane grafted yttria-stabilized zirconia nanocrystals via water/CTAB/hexanol reverse micro-emulsion, Mater. Lett. 61 (2007) 834–836.
[22] C.Y. Tai, M.H. Lee, Y.C. Wu, Control of zirconia particle size by using two-emulsion precipitation technique, Chem. Eng. Sci. 56 (2001) 2389–2398.
[23] C.Y. Tai, B.Y. Hsiao, Characterization of zirconia powder synthesized via reverse microemulsion precipitation, Chem. Eng. Commun. 192 (2005) 1525–1540.
[24] W. Pyda, K. Haberko, M.M. Bucko, Hydrothermal crystallization of zirconia and zirconia solid solution, J. Am. Ceram. Soc. 74 (1991) 2622–2629.
[25] G. Dell'Agli, G. Mascolo, Hydrothermal synthesis of ZrO_2–Y_2O_3 solid solutions at low temperature, J. Eur. Ceram. Soc. 20 (2000) 139–145.
[26] E.K. Goharshadi, S. Samiee, P. Nancarrow, Fabrication of cerium oxide nanoparticles: characterization and optical properties, J. Colloid Interface Sci. 356 (2011) 473–480.
[27] J.C. Debsikdar, Thermal evolution of alkoxy-dertved glass-like transparent zirconia gel, J. Non-Cryst. Solids 87 (1986) 343–349.
[28] M. Shirkhanzadeh, Electrochemical fabrication of alkoxy-derived nanocrystalline zirconia coatings at room temperature, Mater. Lett. 16 (1993) 189–193.
[29] T. Omata, Y. Goto, S. Otsuka-Yao-Matsuo, Nanocrystals of zirconia- and ceria-based solid electrolytes: syntheses and properties, Sci. Technol. Adv. Mater. 8 (2007) 524–530.
[30] D. Ciuparu, A. Ensuque, G. Shafeev, F. Bozon-Verduraz, Synthesis and apparent bandgap of nanophase zirconia, J. Mater. Sci. Lett. 19 (2000) 931–933.
[31] C. Corbella, M. Vives, A. Pinyol, I. Porqueras, C. Person, E. Bertran, Influence of the porosity of RF sputtered Ta_2O_5 thin films on their optical properties for electrochromic applications, Solid State Ionics 165 (2003) 15–22.
[32] F.Z. Tepehan, F.E. Ghodsi, N. Ozer, G.G. Tepehan, Optical properties of sol–gel dip-coated Ta_2O_5 films for electrochromic applications, Sol. Energy Mater. Sol. Cells 59 (1999) 265–272.
[33] S.Q. Zhou, R. Ni, D. Funsehilling, Effects of shear rate and temperature on viscosity of alumina polyalphaolefins nanofluids, J. Appl. Phys. 107 (2010), 054317/1–054323/6.
[34] H. Chen, Y. Ding, Y. He, C. Tan, Rheological behaviour of ethylene glycol based titania nanofluids, Chem. Phys. Lett. 444 (2007) 333–337.
[35] H. Chen, Y. Ding, C. Tan, Rheological behaviour of nanofluids, New J. Phys. 9 (2007), 367/1–367/24.